Article

Effect of Threading Dislocations on the Electronic Structure of La-Doped BaSnO₃ Thin Films

Jeonghun Kang [1], Jeong Hyuk Lee [1], Han-Koo Lee [2], Kwang-Tak Kim [1], Jin Hyeok Kim [3], Min-Jae Maeng [4], Jong-Am Hong [4], Yongsup Park [4,5] and Kee Hoon Kim [1,6,*]

[1] Center for Novel States of Complex Materials Research, Department of Physics and Astronomy, Seoul National University, Seoul 08826, Korea; kangjh1127@snu.ac.kr (J.K.); xaaer5@snu.ac.kr (J.H.L.); kgtakee@snu.ac.kr (K.-T.K.)

[2] Pohang Accelerator Laboratory, Pohang University of Science and Technology, Pohang 37673, Korea; hangulee@postech.ac.kr

[3] Optoelectronic Convergence Research Center, Department of Materials Science and Engineering, Chonnam National University, Gwangju 61185, Korea; jinhyeok@chonnam.ac.kr

[4] Department of Physics, Kyung Hee University, Seoul 02447, Korea; dut0618@khu.ac.kr (M.-J.M.); elavian@khu.ac.kr (J.-A.H.); parky@khu.ac.kr (Y.P.)

[5] Department of Information Display, Kyung Hee University, Seoul 02447, Korea

[6] Department of Physics and Astronomy, Institute of Applied Physics, Seoul National University, Seoul 08826, Korea

* Correspondence: khkim@phya.snu.ac.kr

Abstract: In spite of great application potential as transparent *n*-type oxides with high electrical mobility at room temperature, threading dislocations (TDs) often found in the (Ba,La)SnO₃ (BLSO) films can limit their intrinsic properties so that their role in the physical properties of BLSO films need to be properly understood. The electrical properties and electronic structure of BLSO films grown on SrTiO₃ (001) (STO) and BaSnO₃ (001) (BSO) substrates are comparatively studied to investigate the effect of the TDs. In the BLSO/STO films with TD density of ~1.32×10^{11} cm^{-2}, *n*-type carrier density n_e and electron mobility are significantly reduced, as compared with the BLSO/BSO films with nearly no TDs. This indicates that TDs play the role of scattering-centers as well as acceptor-centers to reduce *n*-type carriers. Moreover, in the BLSO/STO films, both binding energies of an Sn 3*d* core level and a valence band maximum are reduced, being qualitatively consistent with the Fermi level shift with the reduced *n*-type carriers. However, the reduced binding energies of the Sn 3*d* core level and the valence band maximum are clearly different as 0.39 and 0.19 eV, respectively, suggesting that the band gap renormalization preexisting in proportion to n_e is further suppressed to restore the band gap in the BLSO/STO films with the TDs.

Keywords: perovskite oxide; barium stannate (BaSnO3); photoemission spectroscopy; threading dislocation; bandgap renormalization

1. Introduction

In recent years, the perovskite stannate BaSnO₃ (BSO) system with donor-doping (e.g., La³⁺) has received considerable attention due to its high electron mobility (μ_e), high electrical conductivity (σ), high optical transparency, and excellent thermal/chemical stability. Moreover, with the control of La³⁺ doping levels, the BSO system can play versatile roles of either transparent semiconductors or transparent conductors. Various transparent electronic devices employing the La-doped BSO (Ba$_{1-x}$La$_x$SnO₃, BLSO) have been demonstrated: active *n*-channel materials in the *p-n* junctions [1] and the field-effect transistors (FETs) [2], sensitive UV photoconductors [3], and electron transport layers in perovskite solar cells [4].

Among the various forms of BLSO, single crystals have so far exhibited the highest μ_e~320 cm²/V·s and the highest σ~2 × 10⁴ S/cm at room temperature. To find the origin

of these superior electrical characteristics, the band structure of the BLSO film has been intensively investigated both theoretically and experimentally. The indirect nature of the bandgap ~3.1 eV and conduction band filling of the BLSOs were observed by various experimental procedures such as X-ray photoemission spectroscopy (XPS), optical spectroscopy, and ellipsometry [5–7]. Corroborating the experimental results, several recent calculations on the band structures of BLSO with density functional theory (DFT) combined with the hybrid functions predict that the La-doping into BSO results in a degenerate semiconductor with an indirect bandgap of ~3.1 eV [8–11]. Moreover, typical behavior of the degenerate semiconductor such as the Burstein–Moss shift and band gap renormalization was observed in the BLSO films [6]. Both theoretical and experimental investigations indicate that the superior electrical characteristics mainly stem from two intrinsic physical properties. First, the BSO allows the degenerate-doping of La^{3+} ions into a highly dispersive conduction band, mainly composed of Sn $5s$ orbitals, allowing a full activation of donors and a small effective mass of electron carriers. Secondly, a high dielectric constant (~20) of BSO leads to the suppressed ionic dopant scattering, resulting in a high μ_e [11].

However, the electrical properties of BLSO films are often inferior to those of single crystals. For example, the BLSO films grown on the $SrTiO_3$ (STO) (001) substrate, having a lattice mismatch of about ~-5.4%, exhibit a typical μ_e~10–70 $cm^2/V \cdot s$ [12]. This is mainly due to the additional carrier scattering coming from the various types of defects or dislocations, i.e., oxygen vacancies, Ba/Sn antisites, Ruddlesden–Popper shear faults, and threading dislocations (TDs) [13–18]. To envision further improvement of the μ_e of the BLSO films, it is thus essential to control the various types of defects and understand the role of such defects in the physical properties of the films.

Toward the end of realizing the films with higher μ_e, there have been various experimental efforts such as different growth methods, the use of buffer layers and substrates with reduced lattice mismatch, and post-treatment. All of those efforts have so far resulted in the highest achievable μ_e~70–183 $cm^2/V \cdot s$ [13–18], which are overall improved but still scattered. As an example relevant to the present study, Mun et al. [19] controlled the growth temperature of $Ba_{0.96}La_{0.04}SnO_3$/STO (001) films and revealed that μ_e is enhanced when TD density (N_D) is reduced. Furthermore, with the control of the post-annealing condition at Ar and H_2 atmosphere, Yoon et al. [20] similarly observed that the μ_e of $Ba_{1-x}La_xSnO_3$/MgO (001) films, having a lattice mismatch of ~$+2.2\%$ between $a_{BSO} = 4.116$ Å and $a_{MgO} = 4.212$ Å, is proportional to $1/N_D$. The highest μ_e at room temperatures achieved in those studies were ~70 $cm^2/V \cdot s$ ($n_e = 4.0 \times 10^{20}$ cm^{-3}) [19] and 120 $cm^2/V \cdot s$ ($n_e = 1.1 \times 10^{20}$ cm^{-3}) [20], respectively. Both studies have thus suggested a critical role of TD in limiting μ_e. On that account, controlling TD seems to be crucial for improving the μ_e of the BLSO films.

The actual μ_e should also be affected by other defect sources, which were simultaneously created by either growth temperatures, annealing atmosphere, or the La^{3+} dopant concentration. For example, Yoon et al. [20] observed from the XPS study of the O 1s core level that extra oxygen vacancies were formed in the BLSO films upon being post-annealed under H_2 gas. Moreover, Cho et al. [21] observed that extra oxygen vacancies were created with increasing La^{3+} dopant concentration from the XPS study of the O 1s core level. Therefore, understanding the pure effects of the TD only on the transport properties is a challenging task. Moreover, how the electronic structures of BLSO films are affected by the TD has not been fully understood either as the specimens with the TD only are still lacking.

In this regard, the use of a $BaSnO_3$ (BSO) (001) substrate (with a lattice mismatch < 0.03%) in the growth should be one of the most effective ways to achieve the BLSO film without TD. In our former study [15], a $Ba_{0.99}La_{0.01}SnO_3$ film grown on BSO (001), subsequently followed by in-situ O_2 annealing, resulted in no TD, μ_e~100 $cm^2/V \cdot s$ and $n_e = 1.3 \times 10^{20}$ cm^{-3} at room temperature. On the other hand, upon the same growth and in-situ annealing conditions being applied, a $Ba_{0.99}La_{0.01}SnO_3$/STO (001) film showed μ_e~25 $cm^2/V \cdot s$ and $n_e = 5.8 \times 10^{19}$ cm^{-3} [22]. These two BLSO films grown on BSO (001) and STO (001) with the same La^{3+} dopant concentration and growth/annealing condition are thus expected to be useful for comparing the physical properties of the BLSO films with or without TDs.

In this work, we investigate the role of TD on the electrical properties and electronic band structure of the BLSO films. To have the two kinds of films with or without TDs, the BLSO films with 0.5%, 1%, and 4% La doping are grown under identical growth and annealing conditions on two different substrates, BSO (001) (a = 4.116 Å) and STO (001) (a = 3.905 Å). Through the use of the BSO (001) substrate, the BSLO films without TDs are successfully obtained. Therefore, these two sets of BLSO films grown on STO (001) and BSO (001) could be an interesting platform to trace the intrinsic effect of TDs on their transport properties and electronic structures.

2. Materials and Method

2.1. Sample Preparation

$Ba_{1-x}La_xSnO_3$ films with x = 0.005, 0.01, and 0.04, all of which having a thickness t = ~80 nm, were grown on the BSO (001) and the STO (001) substrate by the pulsed laser deposition (PLD) method, the growth conditions of which have been reported previously [15]. Stoichiometric dense polycrystalline pellets of $Ba_{1-x}La_xSnO_3$ with x = 0.005, 0.01, and 0.04 were synthesized to be used as the target material in the PLD process. To minimize the variation of the film quality, the films were grown under the same experimental conditions: a 10 Hz repetition rate by the KrF laser (wavelength 248 nm), laser fluence of 0.7 J/cm^2, oxygen partial pressure of 100 mTorr, and the substrate temperature of 790 °C.

A commercial STO (001) (MTI Corp., Richmond, VA, USA, t = 0.5 mm) and a custom-made BSO (001) single crystal were used as the substrates. The BSO single crystal was grown by the flux method using the mixture of CuO and CuO_2 as a flux, as described in our previous report [15]. Then, the (001) surface of the as-grown BSO crystal was polished using a commercial polishing machine (Allied #70-1218) with polishing cloths and colloidal silica suspension to achieve a smooth surface. The polished BSO (001) substrate exhibited excellent crystallinity as indicated by the full width at half maximum (FWHM) of 0.022° in the ω-rocking curve of the (002) peak. Moreover, the root-mean-square roughness of 0.09 nm was achieved after polishing to prove an atomically smooth surface [15].

2.2. Structure and Electrical Properties Analysis

The structural properties of the BLSO films were investigated by the reciprocal space mapping (RSM) using high-power X-ray diffractometers (Empyrean^{TM}, PANalytical, Malvern, UK). All the RSM data in this study were measured near the BLSO (103) peak. To visualize the TD, transmission electron microscope (TEM) images (JEM-3000F, JEOL, Tokyo, Japan) were obtained in the two $Ba_{0.96}La_{0.04}SnO_3$ films grown on STO (001) and BSO (001). Electronic properties including resistivity (ρ), n_e, and μ_e were investigated by the Hall effect measurement system (HL5500PC, Bio-Rad, Bend, OR, USA) with Van der Pauw contacts at room temperature. To ensure ohmic contact, Ti (thickness t = 5 nm) and Au (t = 50 nm) electrodes were sequentially deposited by a custom-made thermal evaporator.

2.3. Photoemission Spectroscopy Measurement

To investigate the electronic structure of BLSO films, ultraviolet photoemission spectroscopy (UPS) and XPS based on the synchrotron radiation source were performed at the Pohang Accelerator Laboratory (PLS-II4D, photoemission beamline). Each sample was electrically connected to the ground by using a carbon tape to prevent the surface charging effects. Inside the chamber with the ultra-high-vacuum condition, each sample was then etched with Ar plasma for ~30 s to remove surface contamination. Before XPS and UPS measurements, to achieve accurate electron binding energy (E_B), the work function of the spectrometer was calibrated using the Au reference. Photon energies used for XPS and UPS were 650 eV and 90 eV, respectively.

3. Result and Discussion

In our previous study [15], it was established that $Ba_{1-x}La_xSnO_3$ (x = 0.00–0.04) films with t = ~90 nm could be epitaxially grown on the BSO (001) substrate without any

dislocation and with minimized strain development. On the other hand, those grown on STO films with t = ~100 nm have exhibited many TDs with fully relaxed strains [19]. Here, with nearly the same growth conditions, including the same oxygen partial pressure and temperatures, we have grown the $Ba_{1-x}La_xSnO_3$ (x = 0.005, 0.01, and 0.04) films on the two kinds of substrates, STO (001) and BSO (001). Moreover, we have also fixed t = 80 nm in both sets of films as the transport properties are known to be also varied by thickness [23] via, e.g., strain. In this way, we presume that the transport and the electronic structure can be most affected by the TD, and the influences by other defects or strains can be minimized.

Figure 1 presents the RSM data measured in the $Ba_{1-x}La_xSnO_3$ (x = 0.005, 0.01, and 0.04) films grown on STO (001) and BSO (001). The RSM data in Figure 1a–c show that the BLSO (103) peak is well separated from the STO (103) peak, which directly supports the fully relaxed strains across the BLSO/STO films, regardless of the La doping ratio. On the other hand, as found in Figure 1d–f, the BLSO (103) peaks of the BLSO/BSO films are located at almost the same reciprocal positions with the corresponding peaks of BLSO/STO films. Moreover, they overlapped well with the BSO (103) peak so that they are not even distinguishable from the BSO (103) peak. Note that the BLSO/BSO (103) peaks are slightly elongated along the Q_z direction as the La doping ratio x increases. However, such a small strain variation within t = 80 nm is not likely to affect the transport properties significantly. All these observations in the RSM data thus support the conclusion that the nearly perfect in-plane lattice match resulted in the BLSO/BSO films with minimal effect of strain variation, and their lattice constants are similar to those of BLSO/STO films.

To visualize the possible TD and estimate its areal density N_D, a cross-sectional TEM study was performed, particularly in the $Ba_{0.96}La_{0.04}SnO_3$ films grown on STO (001) and BSO (001) substrates (Figure 2a,b). The TDs can be easily identified as dark lines in the TEM image of the BLSO/STO (Figure 2a, red arrows). To extract N_D, we have counted the number of TDs with more than 50 % thickness in a wide range TEM image (Figure S1). The number is then divided by a lateral dimension of the image to calculate the line density, of which square was used to estimate the areal density N_D as ~1.32×10^{11} cm^{-2}. Note that N_D is, in principle, expected to be varied with the lattice constant variation of the film. However, as the lattice constants of the three BLSO films (x = 0.005, 0.01, and 0.04) are nearly the same within 0.03%, which is also obvious in the RSM data in Figure 1a–c, the N_D values of the other $Ba_{1-x}La_xSnO_3$/STO films (x = 0.005 and 0.01) are likely similar to that of the $Ba_{0.96}La_{0.04}SnO_3$/STO film.

In sharp contrast to the $Ba_{0.96}La_{0.04}SnO_3$/STO films, no TDs can be found in the $Ba_{0.96}La_{0.04}SnO_3$/BSO film, as is evident in Figure 2b. This is understood to be due to the nearly perfect in-plane lattice match between the film and the substrate. Therefore, a comparison of physical properties in the two sets of BLSO films grown on BSO and STO substrates with t = 80 nm can be suitable to understand the effect of TD with a relatively low strain effect involved. We emphasize again that in all the RSM data of Figure 1, the center position of each BLSO/BSO (103) peak is very close to the corresponding center position of the BLSO/STO (103) peak. This indicates that the physical properties within the BLSO grains at least could be similar to each other, regardless of the substrate used.
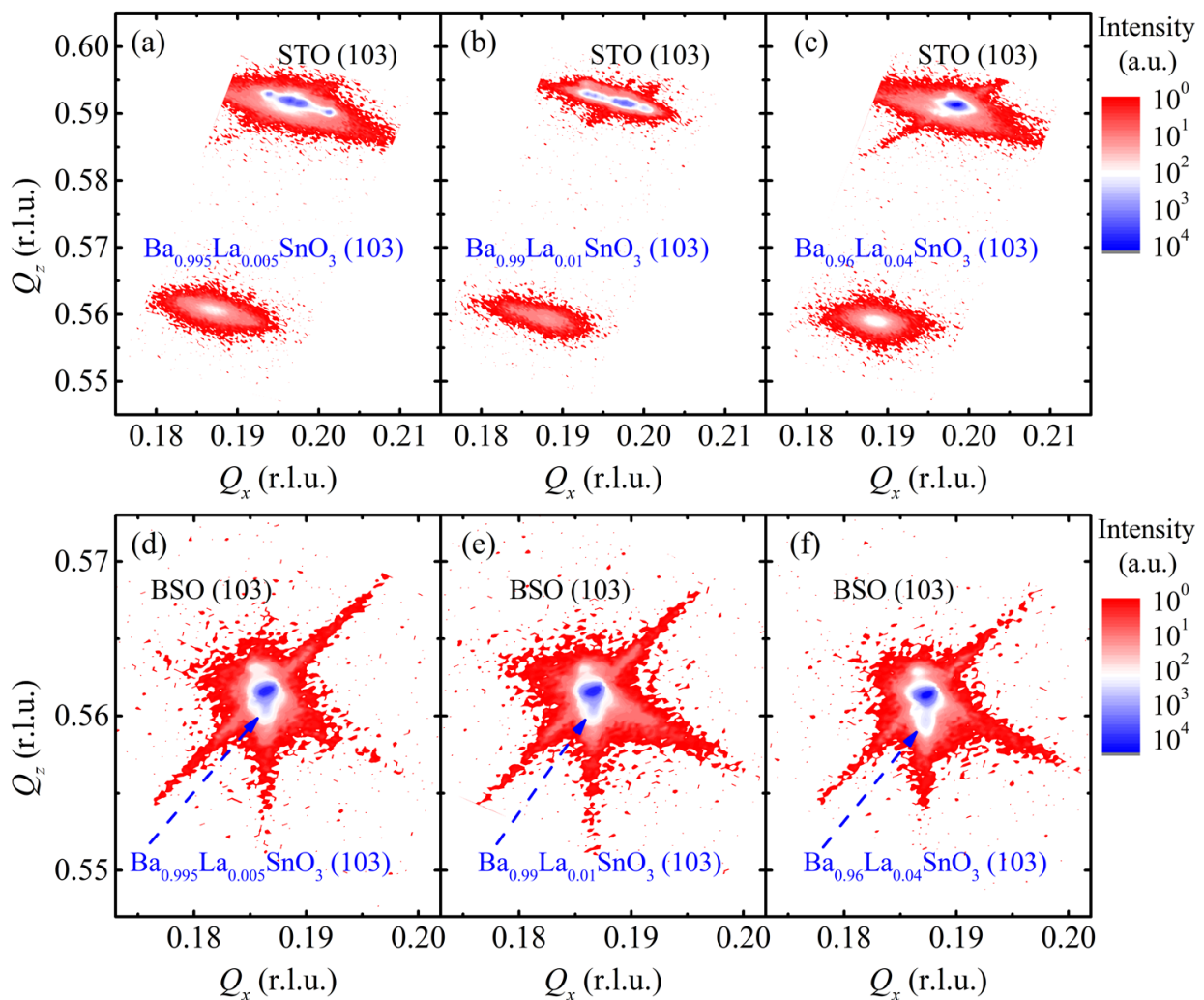
Figure 1. The reciprocal space mapping (RSM) data of $Ba_{1-x}La_xSnO_3$ (x = 0.005, 0.01, 0.04) films grown on (**a–c**) STO (001) and (**d–f**) BSO (001) subtrates, all of which were taken near the (103) peaks.
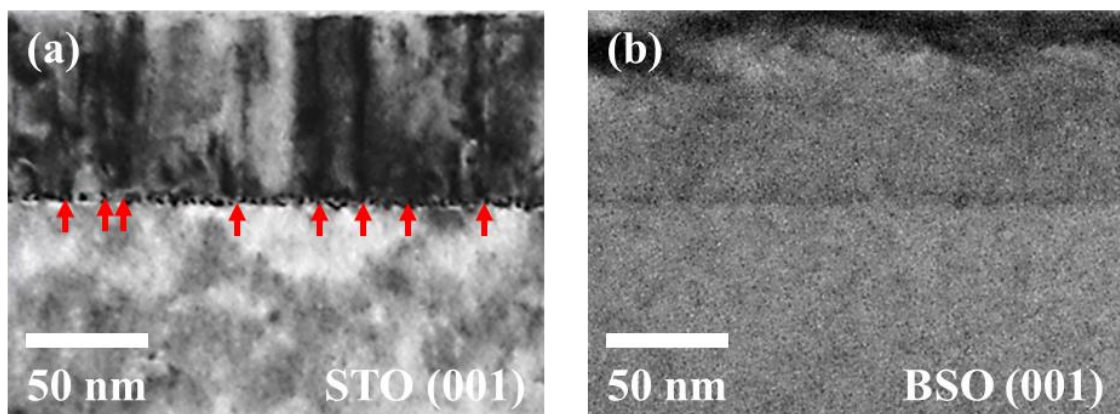

Figure 2. Transmission electron microscope (TEM) images of $Ba_{0.96}La_{0.04}SnO_3$ film deposited on (**a**) STO (001) and (**b**) BSO (001) substrates. Red arrows in (**a**) indicate the TDs.

Figure 3 compares the electrical properties of the BLSO films with various La doping ratios (x = 0.005, 0.01, and 0.04), grown on both STO (001) and BSO (001) substrates. Note that the electrical properties of the $Ba_{0.995}La_{0.005}SnO_3$/STO film could not be measured due to its high resistivity. In Figure 3, two major systematic behaviors can be identified. For

all x, BLSO/STO films exhibit lower n_e and μ_e as compared with BLSO/BSO films. These experimental findings indicate that the electrical properties of BLSO films are affected by the TDs in two ways. First, TDs act as acceptor-centers and thus reduce n_e. Secondly, TDs provide extra scattering centers and thus reduce μ_e. A similar reduction of μ_e limited by the dislocation was also reported in the other BLSO films ($\mu_e \sim N_D^{-1}$) [20] and binary semiconductors such as GaN and GaAs [24].
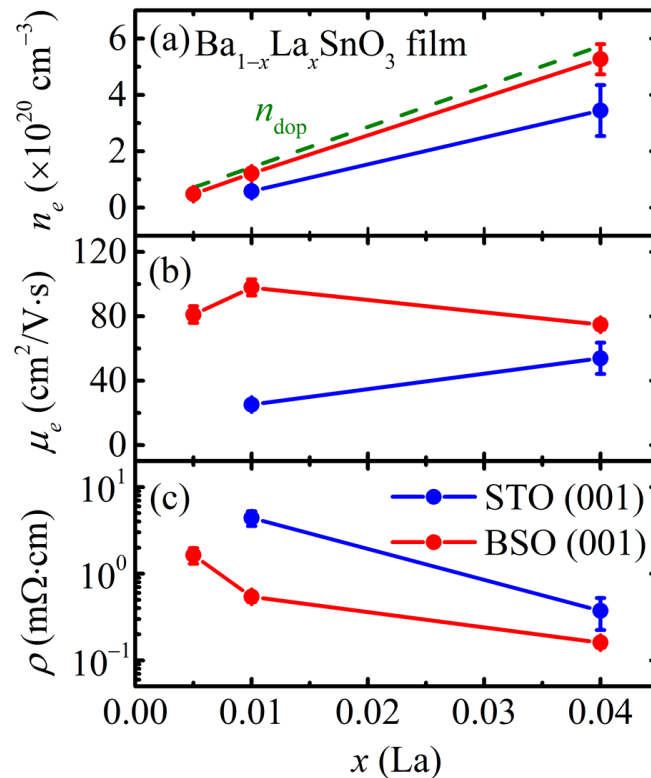

Figure 3. (**a**) Electron concentration (n_e), (**b**) electron mobility (μ_e), and (**c**) resistivity (ρ) of the Ba$_{1-x}$La$_x$SnO$_3$ films grown on BSO (001) (red solid symbols) and STO (001) (blue solid symbols) substrates. A green dotted line in (**a**) indicates a nominal dopant concentration (n_{dop}) expected from the fully activated La^{3+} dopant.

The reduced n_e and μ_e in the BLSO/STO films can be explained by the role of dangling bonds existing at TDs. The periodic lattice structure of the BLSO film is expected to be discontinued at the TDs, which can naturally lead to the dangling bonds in the atoms located at the dislocation sites. These dangling bonds can then attract free electrons near the TDs and trap them into their bonding sites, thus resulting in much reduced n_e as compared with that of the BLSO/BSO films (Figure 3a). From the TEM image in Figure 2a, one can assume that each TD can be approximately modeled as a square rod with a height of 80 nm and width of 10 nm, which results in ~1.89×10^4 dangling bonds per one TD if each unit cell contains one dangling bond. With the observed $N_D = 1.32 \times 10^{11}$ cm^{-2}, a maximum reduced n_e of 3.12×10^{20} cm^{-3} is then expected for the Ba$_{0.96}$La$_{0.04}$SnO$_3$/STO film (see Supplementary Information for details). Note that the experimental value of the reduced n_e in Figure 3a is 2.29×10^{20} cm^{-3} for the La 4% specimen, which is roughly consistent with the estimated value. Furthermore, upon the free electrons' being trapped, the TD sites should become negatively charged. Due to repulsive interaction between negatively charged dislocation sites and free electrons, extra ionic scattering is expected to occur in the electron transport process, thereby resulting in the decrease of μ_e as observed in the BLSO/STO films (Figure 3b).

It should be noted that, as presented in Figure 3a, BLSO/BSO films have nearly similar carrier concentrations with a nominal dopant concentration (n_{dop}) (green dashed line). n_{dop}

is the expected carrier concentration when the donors were fully activated by substitution of La^{3+} for Ba^{2+} ions. This observation supports the good overall stoichiometry of our films, producing nearly expected carrier concentrations as the target materials. Though, a slightly lower n_e could indicate that another source of acceptor-centers other than TDs might exist in the BLSO/BSO films. Paik et al. suggested that the Ruddlesden–Popper crystallographic shear faults might also act as acceptor-centers [16].

To investigate the electronic structure of the BLSO films, both UPS and XPS were employed. The UPS and XPS spectra represent the filled electronic density of states (DOS) as a function of energy below the Fermi energy level (E_F). Due to a low photon energy, ~90 eV, the UPS is an ideal probe to investigate the DOS of the valence band near the E_F. Figure 4a presents the UPS spectra as a function of E_B, showing the valence bands of $Ba_{0.96}La_{0.04}SnO_3$/BSO and $Ba_{0.96}La_{0.04}SnO_3$/STO films comparatively. It is worth noticing in Figure 4a that the valence band of $Ba_{0.96}La_{0.04}SnO_3$/STO is shifted to the lower E_B as compared to that of $Ba_{0.96}La_{0.04}SnO_3$/BSO. To quantify the valence band shift, the valence band maximum (VBM) was determined as the intercept of the E_B axis with a linearly extrapolated line on the steeply increasing valence band tails (dashed lines in Figure 4a). The VBM determined by this method represents the E_B at the valence band edge of the BLSO films. Therefore, the E_B of VBM should decrease/increase when the valence band is shifted toward/away from the E_F.
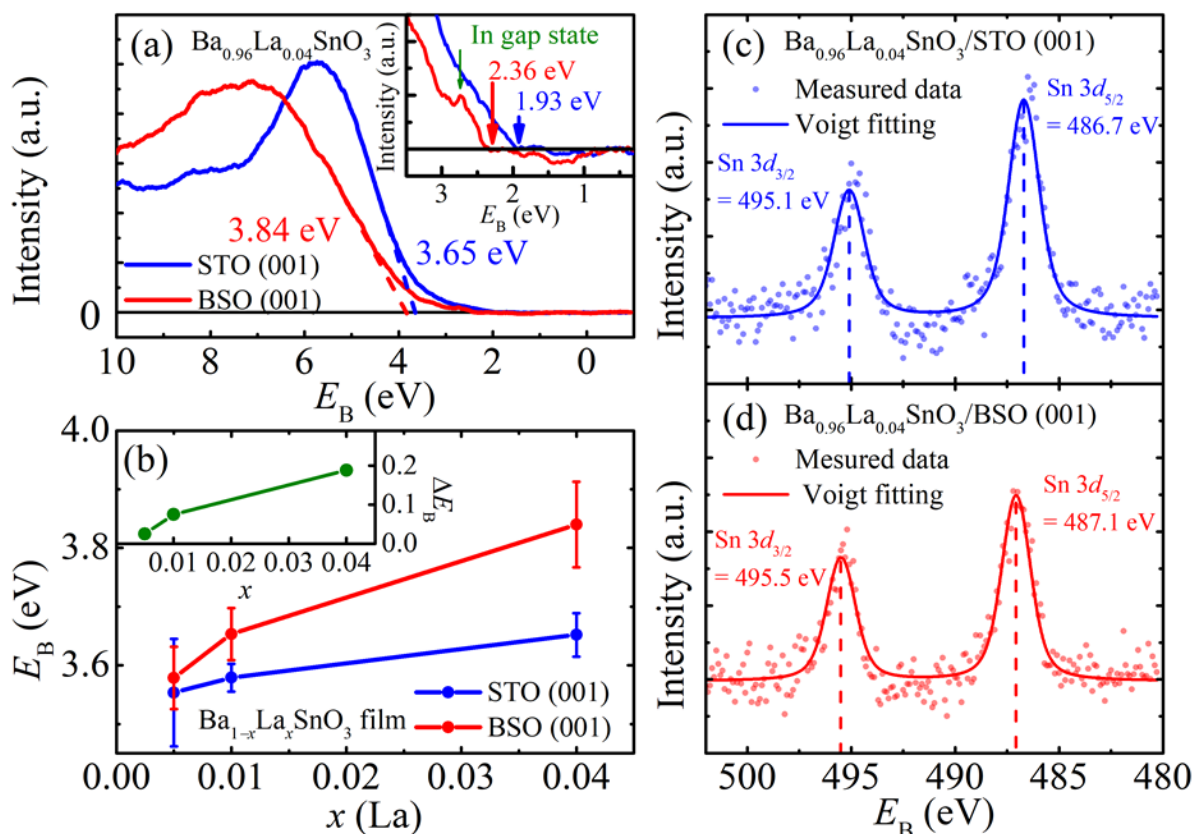

Figure 4. (**a**) The UPS spectra of $Ba_{0.96}La_{0.04}SnO_3$ films grown on STO (001) (blue lines) and BSO (001) (red lines) substrates. The inset shows the same UPS spectrum enlarged near the tail. (**b**) A summary of E_B's of the valence band maximum (VBM) estimated from the UPS spectra of BLSO films grown on both STO (blue) and BSO (red) substrates. The inset shows the VBM difference between the BLSO films grown on BSO (001) and STO (001) substrates (**c,d**) XPS spectra near the Sn 3*d* core level in $Ba_{0.96}La_{0.04}SnO_3$ films grown on STO (001) (blue) and BSO (001) (red). Scattered symbols represent the measured data, and the solid lines are the fitted curves by the Voigt profile. Dashed lines in (**c,d**) indicate the peak positions of each spectrum.

As a degenerate semiconductor, the E_F of the BLSO should be located well inside the conduction band, which is known to be mainly composed of Sn 5s orbitals. However, in our UPS study, the filled states from the conduction band structure of the BLSO films could not be identified (see the expanded spectra in the inset of Figure 4a). On the other hand, photoemission spectra corresponding to the filled states from the conduction band of the BLSO films were observed experimentally at E_B~0.5 eV in several hard X-ray photoemission spectroscopy (HAXPES) studies [6,7]. In general, the ratio of photoionization cross-section between Sn 5s orbital and O 2p orbital decreases exponentially with decreasing photon energy. Considering that the photon energy (~90 eV) used in the UPS measurement is ~10 times lower than that of typical HAXPES measurements, conduction electron states are not likely observable due to the low photoemission intensity of the Sn 5s orbital as compared to the O 2p orbital.

In the inset of Figure 4a, the UPS spectrum of $Ba_{0.96}La_{0.04}SnO_3$/BSO film shows a peak near the tail region around ~2.75 eV. This peak is suspected to represent the DOS of the in-gap state attributable to various defects in the BLSO film (i.e., La^{3+} donor, oxygen vacancies, etc.) [5]. Even though BLSO/BSO films have no TD, other defects such as oxygen vacancy can be a source of such in-gap states. In contrast, there is no clear peak feature attributable to the in-gap state in the UPS spectrum of the $Ba_{0.96}La_{0.04}SnO_3$/STO film. Since the $Ba_{0.96}La_{0.04}SnO_3$/STO film has TDs as additional defects, its valence band is shifted toward the E_F so that the edge region of the valence band near 2.75 eV has increased its intensity. Considering the fact that the UPS spectrum of the in-gap state is ~20 times smaller than that of the main valence band region, the in-gap state is expected to be hidden when the in-gap state is located near the valence band edge. Therefore, it is likely that the in-gap state of the $Ba_{0.96}La_{0.04}SnO_3$/STO film is embedded in the band edge spectra.

We have investigated the UPS spectra of other La dopings as well to compare the shifts of VBM in the two sets of BLSO films (Figure S3) and summarized the results in Figure 4b. The VBM shifts of the BLSO films grown on BSO (001) and STO (001) show three major features. First, the E_B of the VBM in BLSO films generally increases with the increase of x. Secondly, BLSO/BSO films exhibit higher E_B's at the VBMs than BLSO/STO films for all the x. Thirdly, the difference of the E_B's at the VBM between the BLSO/BSO and BLSO/STO films increases with x (see the inset of Figure 4b). The first and second behaviors can be simply explained by the E_F shift. Since the E_F of the BLSO films increases with n_e, the E_B of the VBM of BLSO films supposedly increases with n_e. The higher E_B's of the VBMs observed in the BLSO/BSO films compared to the BLSO/STO films are qualitatively consistent with this explanation. Indeed, the $Ba_{0.96}La_{0.04}SnO_3$/BSO film, which has the highest n_e without TD, exhibits the highest E_B of the VBM ~3.84 eV among the BLSO films investigated in this work. Moreover, the increasing tendency with x observed in the VBM difference between the two film sets (inset of Figure 4b) can also be understood as being due to the E_F shift. Since the n_e difference between the BLSO/BSO films and the BLSO/STO film increases with x, as shown in Figure 3a, the VBM difference between the two sets of BLSO films should also increase.

Although the E_F shift can explain the valence band shift of the BLSO films qualitatively, it is questionable whether the E_F shift is sufficient for understanding the effect of TD on the band structure of the BLSO films. To clarify this, we have investigated the core level spectra of the $Ba_{0.96}La_{0.04}SnO_3$ films by XPS. Figure 4c,d shows the Sn 3d core level spectra of $Ba_{0.96}La_{0.04}SnO_3$/BSO and $Ba_{0.96}La_{0.04}SnO_3$/STO, respectively. To determine the center positions of the Sn 3$d_{3/2}$ and the Sn 3$d_{5/2}$ peaks, the spectra were fitted by the Voigt function, which contains both Gaussian and Lorentzian terms to represent instrumental broadening and inherent XPS spectrum, respectively. To determine the instrumental broadening, we measured the XPS spectra of Au metal and fitted the Au 4f peak using the Voigt function with a fixed Lorentzian width (FWHM = 0.29 eV) [25]; the instrumental broadening factor was determined as ~1.26 eV. With the known instrumental broadening factor, the Sn 3$d_{3/2}$ and Sn 3$d_{5/2}$ core level spectra were fitted by the Voigt profile; Table 1 summarizes the fit results.

Table 1. The Sn *3d* core level of La 4% doped BLSO film deposited on STO and BSO substrates.

	Sn $3d_{3/2}$	Sn $3d_{5/2}$	FWHM
$Ba_{0.96}La_{0.04}SnO_3$/STO	495.10 ± 0.11 eV	486.69 ± 0.07 eV	1.77 ± 0.06 eV
$Ba_{0.96}La_{0.04}SnO_3$/BSO	495.49 ± 0.11 eV	487.07 ± 0.07 eV	1.70 ± 0.05 eV

According to Table 1, it is unambiguously found that both the Sn $3d_{3/2}$ and Sn $3d_{5/2}$ core levels of the $Ba_{0.96}La_{0.04}SnO_3$/STO are found at the lower E_B's by ~0.39 eV and ~0.38 eV, respectively, as compared to those of $Ba_{0.96}La_{0.04}SnO_3$/BSO. Moreover, the FWHMs estimated in the XPS spectra of $Ba_{0.96}La_{0.04}SnO_3$/STO and $Ba_{0.96}La_{0.04}SnO_3$/BSO are 1.77 eV and 1.70 eV, respectively. (Note that the same FWHM is assumed for the Sn $3d_{3/2}$ and Sn $3d_{5/2}$ core level spectra.) The FWHM value of the Sn *3d* spectra in the BLSO/BSO film is indeed in good agreement with that obtained previously in an indium tin oxide film (~1.70 eV), while the FWHM value in the BLSO/STO film is slightly larger (~1.77 eV) [26].

Since the BLSO films were connected to a common ground in the UPS and XPS measurements, it is natural to align the band structure with respect to E_F. Figure 5 shows the schematic band structures of $Ba_{0.96}La_{0.04}SnO_3$/BSO and $Ba_{0.96}La_{0.04}SnO_3$/STO aligned with respect to E_F. Figure 5a,b shows that both the Sn $3d_{3/2}$ core level and the valence band in the $Ba_{0.96}La_{0.04}SnO_3$/STO film are shifted to lower E_B by ΔE_{Sn} ~0.39 eV and ΔE_{VBM} ~0.19 eV, respectively. If the E_F shift had only occurred with the TDs, ΔE_{Sn} and ΔE_{VBM} would have been nearly the same as described in Figure 5c. Therefore, experimental observation of different ΔE_{VBM} and ΔE_{Sn} suggests that the origin of their shift should be explained separately.
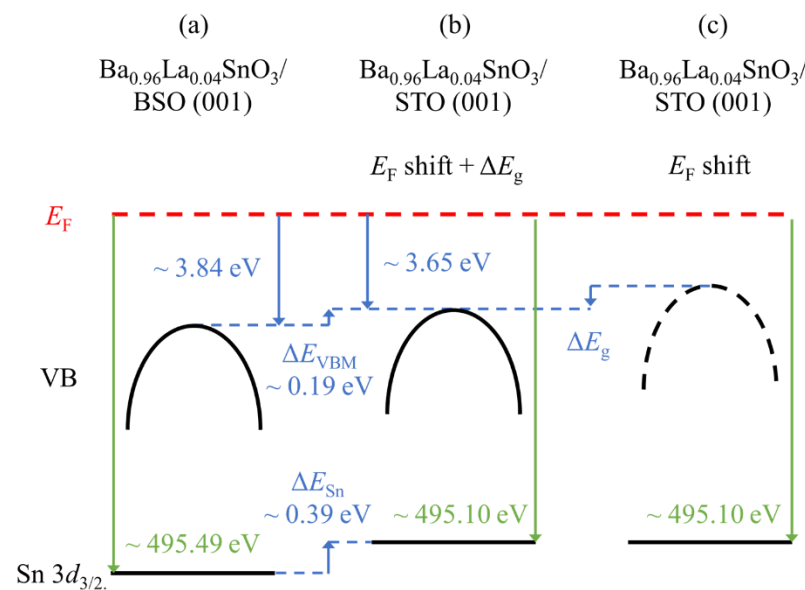

Figure 5. Schematic electronic band structures of (**a**) $Ba_{0.96}La_{0.04}SnO_3$/BSO (001), (**b**) $Ba_{0.96}La_{0.04}SnO_3$/STO (001) with the E_F shift and the restored band gap (ΔE_g), and (**c**) $Ba_{0.96}La_{0.04}SnO_3$/STO (001) with only the E_F shift. These band schematics include the valence band (VB), its maximum (VBM), and a Sn $3d_{3/2}$ core level (Sn $3d_{3/2}$).

One of the most probable explanations for different ΔE_{VBM} and ΔE_{Sn} is the band gap renormalization effect, which is tied to n_e. The band gap renormalization refers to the shrinking of a band gap proportional to n_e, which is often observed in degenerate semiconductors like the BLSO system [6]. When free electrons are introduced to degenerate semiconductors, conduction bands/valence bands are shifted to a higher/lower E_B, owing to the self-energy effect of added free electrons. Namely, the conduction band is shifted to higher E_B as the self-energy of added free electrons is negative. For the valence band, however, Coulomb interaction between electrons becomes weakened since the Hartree–Fock

exchange is replaced with dynamically screened interaction with added free electrons [27]. As a result, the valence band is shifted to a lower E_B. Therefore, upon n_e's being increased, the band gap is reduced due to the band gap renormalization, while upon n_e's being decreased, the bandgap should be restored. In our case, since the TD provides electron trapping sites and clearly reduces n_e, the bandgap should be restored to make the valence band move to higher E_B in the BLSO/STO films. Hence, due to the combined effect of the lowered E_B coming from the E_F shift (0.39 eV) and the restored band gap (0.20 eV), the net VBM shift (0.19 eV) is smaller than in the case with the E_F shift only (0.39 eV), which results in different energy level shifts in the VBM and the Sn $3d_{3/2}$ core levels, as summarized in Figure 5b.

4. Conclusions

The transport, microstructural properties, and electronic band structure of the BLSO films grown on STO (001) and BSO (001) were comparatively investigated to understand the effect of TDs. TDs in the BLSO films play two major roles. First, due to the dangling bonds present in the TDs, they act as electron-traps. Simultaneously, TDs are negatively charged and provide an extra electron scattering center. As a result, TDs make both μ_e and n_e decrease in the BLSO films.

Decreased carrier density attributed to the TDs affects the overall electronic structure of BLSO/STO films. First, E_F is reduced with reduced n_e. As a result, the E_B's of the valence band maximum and Sn $3d$ core level become reduced. Secondly, the band gap, which is shrunk in proportion to n_e, is restored with the reduced n_e. This phenomenon is likely to result in the differently valued E_B lowering in the Sn core level and in the valence band spectra, as observed in the $Ba_{0.96}La_{0.04}SnO_3$/STO (001).

Although only TDs are mainly discussed in this work, other defects, such as oxygen vacancies, can also act as additional electron traps. However, the effects of the other defects on the electronic structure of BLSO films have not been fully understood yet. By combining the result of this study and further research on other defects, we expect that understanding the roles of the various defects on the physical properties of the BLSO films could be helpful to achieve higher quality BLSO films comparable to the BLSO single crystals.

Author Contributions: Conceptualization, K.H.K.; Formal analysis, J.K., J.H.L., H.-K.L., K.-T.K., J.H.K., M.-J.M., J.-A.H. and Y.P.; Investigation, J.K., J.H.L., H.-K.L., K.-T.K., J.H.K., M.-J.M., J.-A.H. and Y.P.; Resources, J.H.K., Y.P. and K.H.K.; Writing—original draft preparation, J.K. and K.H.K.; Writing—review and editing, J.K., J.H.L., H.-K.L., K.-T.K., J.H.K., M.-J.M., J.-A.H., Y.P. and K.H.K.; Visualization, J.K. and J.H.L.; Supervision, K.H.K.; Project administration, J.K. and K.H.K. All authors have read and agreed to the published version of the manuscript.

Institutional Review Board Statement: Not applicable.

Informed Consent Statement: Not applicable.

Data Availability Statement: Not applicable.

Conflicts of Interest: The authors declare no conflict of interest.

References

1. Lee, J.H.; Lee, W.-J.; Kim, T.H.; Lee, T.; Hong, S.; Kim, K.H. Transparent *p*-CuI/*n*-BaSnO$_{3-\delta}$ Heterojunctions with a High Rectification Ratio. *J. Phys. Condens. Matter.* **2017**, *29*, 384004. [CrossRef] [PubMed]
2. Park, C.; Kim, U.; Ju, C.J.; Park, J.S.; Kim, Y.M.; Char, K. High Mobility Field Effect Transistor Based on BaSnO$_3$ with Al$_2$O$_3$ Gate Oxide. *Appl. Phys. Lett.* **2014**, *105*, 203503. [CrossRef]
3. Lee, Y.; Yoon, D.; Yu, S.; Sim, H.; Park, Y.; Nam, Y.-S.; Kim, K.-J.; Choi, S.-Y.; Kang, Y.; Son, J. Reversible Manipulation of Photoconductivity Caused by Surface Oxygen Vacancies in Perovskite Stannates with Ultraviolet Light. *Adv. Mater.* **2021**, *34*, 2107650. [CrossRef] [PubMed]
4. Shin, S.S.; Yeom, E.J.; Yang, W.S.; Hur, S.; Kim, M.G.; Im, J.; Seo, J.; Noh, J.H.; Seok, S.I. Colloidally Prepared La-Doped BaSnO$_3$ Electrodes for Efficient, Photostable Perovskite Solar Cells. *Science* **2017**, *356*, 167–171. [CrossRef] [PubMed]
5. Joo, B.S.; Chang, Y.J.; Moreschini, L.; Bostwick, A.; Rotenberg, E.; Han, M. Evidence for Indirect Band Gap in BaSnO$_3$ Using Angle-Resolved Photoemission Spectroscopy. *Curr. Appl. Phys.* **2017**, *17*, 595–599. [CrossRef]
6. Lebens-Higgins, Z.; Scanlon, D.O.; Paik, H.; Sallis, S.; Nie, Y.; Uchida, M.; Quackenbush, N.F.; Wahila, M.J.; Sterbinsky, G.E.; Arena, D.A.; et al. Direct Observation of Electrostatically Driven Band Gap Renormalization in a Degenerate Perovskite Transparent Conducting Oxide. *Phys. Rev. Lett.* **2016**, *116*, 027602. [CrossRef]
7. Sallis, S.; Scanlon, D.O.; Chae, S.C.; Quackenbush, N.F.; Fischer, D.A.; Woicik, J.C.; Guo, J.-H.; Cheong, S.W.; Piper, L.F.J. La-Doped BaSnO$_3$ Degenerate Perovskite Transparent Conducting Oxide: Evidence from Synchrotron X-ray Spectroscopy. *Appl. Phys. Lett.* **2013**, *103*, 042105. [CrossRef]
8. Wang, W.; Liang, S.; Ding, K.; Bi, J.; Yu, J.C.; Wong, P.K.; Wu, L. Microwave Hydrothermal Synthesis of MSnO$_3$ (M^{2+} = Ca^{2+}, Sr^{2+}, Ba^{2+}): Effect of M^{2+} on Crystal Structure and Photocatalytic Properties. *J. Mater. Sci.* **2014**, *49*, 1893–1902. [CrossRef]
9. Singh, D.J.; Xu, Q.; Ong, K.P. Strain Effects on the Band Gap and Optical Properties of Perovskite SrSnO$_3$ and BaSnO$_3$. *Appl. Phys. Lett.* **2014**, *104*, 011910. [CrossRef]
10. Kim, B.G.; Jo, J.Y.; Cheong, S.W. Hybrid Functional Calculation of Electronic and Phonon Structure of BaSnO$_3$. *J. Solid State Chem.* **2013**, *197*, 134–138. [CrossRef]
11. Kim, H.J.; Kim, U.; Kim, T.H.; Kim, J.; Kim, H.M.; Jeon, B.-G.; Lee, W.-J.; Mun, H.S.; Hong, K.T.; Yu, J.; et al. Physical Properties of Transparent Perovskite Oxides (Ba,La)SnO$_3$ with High Electrical Mobility at Room Temperature. *Phys. Rev. B* **2012**, *86*, 165205. [CrossRef]
12. Lee, W.-J.; Kim, H.J.; Kang, J.; Jang, D.H.; Kim, T.H.; Lee, J.H.; Kim, K.H. Transparent Perovskite Barium Stannate with High Electron Mobility and Thermal Stability. *Annu. Rev. Mater. Res.* **2017**, *47*, 391. [CrossRef]
13. Shiogai, J.; Nishihara, K.; Sato, K.; Tsukazaki, A. Improvement of Electron Mobility in La:BaSnO$_3$ Thin Films by Insertion of an Atomically Flat Insulating (Sr,Ba)SnO$_3$ Buffer Layer. *AIP Adv.* **2016**, *6*, 065305. [CrossRef]
14. Prakash, A.; Xu, P.; Faghaninia, A.; Shukla, S.; Ager, J.W.; Lo, C.S.; Jalan, B. Wide Bandgap BaSnO$_3$ Films with Room Temperature Conductivity Exceeding 10^4 S cm^{-1}. *Nat. Commun.* **2017**, *8*, 15167. [CrossRef] [PubMed]
15. Lee, W.-J.; Kim, H.J.; Sohn, E.; Kim, T.H.; Park, J.-Y.; Park, W.; Jeong, H.; Lee, T.; Kim, J.H.; Choi, K.-Y.; et al. Enhanced Electron Mobility in Epitaxial (Ba,La)SnO$_3$ Films on BaSnO$_3$(001) Substrates. *Appl. Phys. Lett.* **2016**, *108*, 082105. [CrossRef]
16. Paik, H.; Chen, Z.; Lochocki, E.; Seidner, H.A.; Verma, A.; Tanen, N.; Park, J.; Uchida, M.; Shang, S.; Zhou, B.-C.; et al. Adsorption-Controlled Growth of La-Doped BaSnO$_3$ by Molecular-Beam Epitaxy. *APL Mater.* **2017**, *5*, 116107. [CrossRef]
17. Raghavan, S.; Schumann, T.; Kim, H.; Zhang, J.Y.; Cain, T.A.; Stemmer, S. High-Mobility BaSnO$_3$ Grown by Oxide Molecular Beam Epitaxy. *APL Mater.* **2016**, *4*, 016106. [CrossRef]
18. Sanchela, A.V.; Wei, M.; Lee, J.; Kim, G.; Jeen, H.; Feng, B.; Ikuhara, Y.; Cho, H.J.; Ohta, H. Buffer Layer-Less Fabrication of a High-Mobility Transparent Oxide Semiconductor, La-Doped BaSnO$_3$. *J. Mater. Chem. C* **2019**, *7*, 5797–5802. [CrossRef]
19. Mun, H.; Kim, U.; Kim, H.M.; Park, C.; Kim, T.H.; Kim, H.J.; Kim, K.H.; Char, K. Large Effects of Dislocations on High Mobility of Epitaxial Perovskite Ba$_{0.96}$La$_{0.04}$SnO$_3$ Films. *Appl. Phys. Lett.* **2013**, *102*, 252105. [CrossRef]
20. Yoon, D.; Yu, S.; Son, J. Oxygen Vacancy-Assisted Recovery Process for Increasing Electron Mobility in *n*-Type BaSnO$_3$ Epitaxial Thin Films. *NPG Asia Mater.* **2018**, *10*, 363–371. [CrossRef]
21. Cho, H.J.; Onozato, T.; Wei, M.; Sanchela, A.; Ohta, H. Effects of Vacuum Annealing on the Electron Mobility of Epitaxial La-Doped BaSnO$_3$ Films. *APL Mater.* **2019**, *7*, 022507. [CrossRef]
22. Kim, H.J.; Kim, U.; Kim, T.H.; Mun, H.S.; Jeon, B.-G.; Hong, K.T.; Lee, W.-J.; Ju, C.; Kim, K.H.; Char, K. High Mobility in a Stable Transparent Perovskite Oxide. *Appl. Phys. Express* **2012**, *5*, 061102. [CrossRef]
23. Cho, H.J.; Feng, B.; Onozato, T.; Wei, M.; Sanchela, A.V.; Ikuhara, Y.; Ohta, H. Investigation of Electrical and Thermal Transport Property Reductions in La-Doped BaSnO$_3$ Films. *Phys. Rev. Mater.* **2019**, *3*, 094601. [CrossRef]
24. Ng, H.M.; Doppalapudi, D.; Moustakas, T.D.; Weimann, N.G.; Eastman, L.F. The Role of Dislocation Scattering in I-Type GaN Films. *Appl. Phys. Lett.* **1998**, *73*, 821–823. [CrossRef]
25. Kraut, E.A.; Grant, R.W.; Waldrop, J.R.; Kowalczyk, S.P. Precise Determination of the Valence-Band Edge in X-ray Photoemission Spectra: Application to Measurement of Semiconductor Interface Potentials. *Phys. Rev. Lett.* **1980**, *44*, 1620–1623. [CrossRef]
26. Song, W.; So, S.K.; Cao, L. Angular-Dependent Photoemission Studies of Indium Tin Oxide Surfaces. *Appl. Phys. A* **2001**, *72*, 361–365. [CrossRef]
27. Berggren, K.-F.; Sernelius, B.E. Band-Gap Narrowing in Heavily Doped Many-Valley Semiconductors. *Phys. Rev. B* **1981**, *24*, 1971–1986. [CrossRef]